If the scattered wave attenuates along the $-x$-direction with the factor α, then d can be replaced as $d = e^{-\alpha \delta x} z^{-s}$. When high-order ABC's are used, approximate values of ν_i and α_i are adequate. In fact, one may select these values in a range according to the incident angles and attenuation fact of the wave in the frequency band of interest.

III. Numerical Results

In this paper, we give the reflection coefficient caused by a third-order ABC, which is developed when it is used to analyze a rectangular waveguide WR-28. The results are shown in Fig. 1, together with the results obtained when we use the first-order Mur's ABC and 16-layer PML as comparison. The parameters of the ABC were selected as $\nu_1 = 1.2c$, $\nu = 1.4c$, and $\nu_3 = 1.6c$. The type of PML used was PML(16, P, 0.001).

The ABC has been used to calculate the S-parameters of a rectangular dielectric post in a rectangular waveguide WR-28. The cross section of the post is 4 mm $\times$ 2 mm, and the dielectric constant ϵr is 8.2, as shown in Fig. 2(a). Resonance occurred near the frequency $f = 34$ GHz, and very strong high-order modes were excited. In this case, if the truncated plane is set very close to the discontinuity, the ABC should absorb both the dominant and high-order modes, which is demonstrated in [8]. A fifth-order ABC was applied where the phase velocities were selected as $\nu_1 = 1.2c$, $\nu_2 = 1.4c$, $\nu_3 = 1.6c$, $\nu_4 \gg c$, $\nu_5 \gg c$, and the attenuation factors were selected as $\alpha_1 \delta x = 0$, $\alpha_2 \delta x = 0$, $\alpha_3 \delta x = 0$, $\alpha_4 \delta x = 0.02$, $\alpha_5 \delta x = 0.05$. Better results were obtained when the distance between the ABC and discontinuity is 3 mm, as shown in Fig. 2(b)–(d). Since the ordinary PML cannot absorb the high-order (cutoff) modes adequately, it fails to obtain correct results unless the distance is much larger. Our ABC can obtain reasonable results even if the distance is very small, and the computational memory and time can be greatly saved. Since the derivation is not limited two-dimensionally, the ABC can be applied in a three-dimensional (3-D) problems.

IV. Conclusion

In this paper, we use transfer functions to construct ABC's for the first time. Recurrence formulas for the transfer functions and coefficients of the final FD schemes of the ABC's are developed. It is quite simple and convenient to apply the ABC's in the FDTD iteration. A lot of computational time and memory can be saved with the ABC's. Numerical results show the good absorbing performance of the ABC in practical problems.

References

[1] K. S. Yee, "Numerical solution for initial boundary value problems involving Maxwell's equations in isotropic media," *IEEE Trans. Antennas Propagat.*, vol. AP-14, pp. 302–307, May 1966.

[2] B. Engquist and A. Majda, "Absorbing boundary conditions for the numerical simulation of waves," *Math. Comput.*, vol. 31, pp. 629–651, July 1977.

[3] G. Mur, "Absorbing boundary conditions for the finite-difference approximation of the time-domain electromagnetic field equations," *IEEE Trans. Electromag. Compat.*, vol. EC-23, pp. 377–382, Nov. 1981.

[4] Z. Q. Bi, K. Wu, C. Wu, and J. Litva, "A dispersive boundary condition for microstrip component analysis using the FDTD method," *IEEE Trans. Microwave Theory Tech.*, vol. 40, pp. 774–777, 1992.

[5] P. Zhao, J. Litva, and K. Wu, "A new stable and very dispersive boundary condition for the FDTD method," in *Proc. IEEE MTT-S Int. Symp.*, vol. 1, San Diego, CA, May 23–27, 1994, pp. 35–38.

[6] J. P. Berenger, "A perfect matched layer for the absorption of electromagnetic waves," *J. Comput. Phys.*, pp. 185–200, Feb. 1994.

[7] R. L. Higdon, "Absorbing boundary conditions for difference approximations to the multi-dimensional wave equation," *Math. Comput.*, vol. 47, no. 176, pp. 473–459, Oct. 1986.

[8] J. Zhou and W. Hong, "A super absorbing boundary condition for the analysis of waveguide discontinuities with the finite-difference method," *IEEE Microwave Guided Wave Lett.*, vol. 7, pp. 147–149, June 1997.

Edge-Element Formulation of Three-Dimensional Structures

Jilin Tan, Guangwen Pan, and Barry K. Gilbert

***Abstract*—A three-dimensional (3-D) asymmetrical functional is developed and implemented as a hybrid-vector edge-element method. The equivalent frequency-dependent circuit parameters are then extracted from the field solutions. Laboratory measurements and data comparison with previous published results strongly support the newly developed theoretical work.**

***Index Terms*—Edge element, functional.**

I. Introduction

In this paper, we have developed a new functional for general three-dimensional (3-D) guided-wave structures, which need not have completely closed metallic walls. We shall then derive the termination conditions at the planes of incidence and transmittance. Utilizing prior information of the eigenmodes resulting from the evaluation of the two-and-one-half-dimensional edge-element solver [1], the 3-D field solutions are obtained. The frequency-dependent circuit parameters (such as L, C, R, and G) are converted according to relevant equivalent circuits of the structures.

II. Basic Theory

We begin with the vector-wave-propagation equation

$$\nabla \times \frac{1}{\mu_r} \nabla \times \vec{E} - \vec{\vec{\epsilon}}_r k_0^2 \cdot \vec{E} = -j\omega\mu \vec{J} \quad \text{in } V. \tag{1}$$

The boundary conditions for (1) are

$$\begin{cases} \hat{n} \times \vec{E} = \vec{P}, & \text{on } S_1 \\ \dfrac{1}{\mu_r} \hat{n} \times \nabla \times \vec{E} + \gamma_v \hat{n} \times \hat{n} \times \vec{E} = \vec{V}, & \text{on } S_2. \end{cases} \tag{2}$$

In the previous equations, S_1 is the surface where the boundary condition of the first kind applies, S_2 is the surface where the boundary condition of the third kind applies, and $\gamma_v = jk_0\sqrt{(\epsilon_{rc} - j(\sigma/\omega\epsilon_0)/\mu_{rc})}$, as defined in [1]. In the application of this theory to transmission-line structures and their discontinuities, the field component in the signal-propagation direction is generally nonzero, and the aforementioned boundary conditions are insufficient. On both the incident and transmitted planes, the longitudinal

Manuscript received July 22, 1997; revised July 7, 1998.

J. Tan and G. Pan are with the Electrical Engineering Department, Arizona State University, Tempe 85287-7206 USA.

B. K. Gilbert is with the Special Purpose Processor Development Group, Mayo Foundation, Rochester, MN 55905 USA.

Publisher Item Identifier S 0018-9480(98)08017-X.

0018–9480/98$10.00 © 1998 IEEE

component needs to be treated carefully [2]. Without losing generality, we will employ a typical via structure as an example. On the incident plane O_1 and transmitted plane O_2, the suitable termination condition is found to be

$$\hat{n}\times\nabla\times\vec{E}+\gamma_p\hat{n}\times\hat{n}\times\left[\vec{E}+\frac{\nabla_t E_n}{\gamma_p}\right]=\vec{U}. \tag{3}$$

Generally, the functional is no longer symmetric because of (3). Furthermore, to be consistent with the treatment in the two-and-one-half-dimensional case, and with the expressions that we proposed in [1], the adjoint field should be the field which is incident upon plane O_2 and transmitted through O_1. This adjoint system satisfies

$$\nabla\times\frac{1}{\mu_r}\nabla\times\vec{E}^{\dagger}-\vec{\bar{\epsilon}}_r k_0^2\cdot\vec{E}^{\dagger}=-j\omega\mu\vec{J}^{\dagger},\qquad \text{in } V \tag{4}$$

under the associated boundary conditions

$$\begin{aligned}\hat{n}\times\vec{E}^{\dagger}&=\vec{P}^{\dagger}\\ \frac{1}{\mu_r}\hat{n}\times\nabla\times\vec{E}^{\dagger}+\gamma_v^{\dagger}\hat{n}\times\hat{n}\times\vec{E}^{\dagger}&=\vec{V}^{\dagger}\\ \hat{n}\times\nabla\times\vec{E}^{\dagger}+\gamma_p^{\dagger}\hat{n}\times\hat{n}\times\left[\vec{E}^{\dagger}+\frac{\nabla_t E_n^{\dagger}}{\gamma_p^{\dagger}}\right]&=\vec{U}^{\dagger}.\end{aligned} \tag{5}$$

Suppose that we can find an $\vec{E}_0$ or $\vec{E}_0^{\dagger}$, which satisfies the aforementioned boundary conditions. If we define $\vec{e}=\vec{E}-\vec{E}_0$, $\vec{j}=-j\omega\mu_o\vec{J}$ then the following functional [3]:

$$I=\langle\vec{e}^{\dagger},\hat{L}\vec{e}\rangle-\langle\vec{e}^{\dagger},\vec{j}\rangle-\langle\vec{e},\vec{j}^{\dagger}\rangle \tag{6}$$

can still apply, provided that the assumed known vector $\vec{U}$ is modified to $\vec{U}-\hat{n}\times\hat{n}\times\nabla_t E_n$ and the local potential method is employed. Following similar procedures presented in [4], we may further simplify the functional, yielding

$$\begin{aligned}I=&\int_V\left[\frac{1}{\mu_r}(\nabla\times\vec{E}^{\dagger})\cdot(\nabla\times\vec{E})-k_0^2\vec{E}^{\dagger}\cdot\vec{\bar{\epsilon}}_r\cdot\vec{E}\right]dv\\&+\int_{S_2}\gamma_v(\hat{n}\times\vec{E}^{\dagger})(\hat{n}\times\vec{E})\,ds+\int_{O_1+O_2}\frac{\gamma_p}{\mu_r}(\hat{n}\times\vec{E}^{\dagger})\\&\cdot(\hat{n}\times\vec{E})\,ds+\int_{O_1+O_2}\frac{1}{\mu_r}(\vec{U}_0\cdot\vec{E}^{\dagger}+\vec{U}_0^{\dagger}\cdot\vec{E})\,ds\\&+\int_{S_2}(\vec{V}\cdot\vec{E}^{\dagger}+\vec{V}^{\dagger}\cdot\vec{E})\,ds+j\omega\mu_0\int_V(\vec{j}\cdot\vec{E}^{\dagger}+\vec{j}^{\dagger}\cdot\vec{E})\,dv.\end{aligned} \tag{7}$$

Equation (7) can be verified by using Galerkin's procedure to transform the vector-wave equation into the weak integral form [1]. For the via structure, the incident field can be expressed as $\vec{E}^{\rm in}=\vec{E}^0(x,y)e^{-\gamma_1(z-z_1)}$ on the plane of incidence O_1. Thus,

$$\begin{aligned}\vec{E}&=\vec{E}_t^0(x,y)e^{-\gamma_1(z-z_1)}+\Gamma\vec{E}_t^0(x,y)e^{\gamma_1(z-z_1)}\\&\quad+\vec{E}_z^0(x,y)e^{-\gamma_1(z-z_1)}-\Gamma\vec{E}_z^0(x,y)e^{\gamma_1(z-z_1)}\\&=\vec{E}^{\rm in}+\vec{E}^{re}\end{aligned} \tag{8}$$

where Γ is the reflection coefficient. Consequently, on this surface, we obtain

$$\hat{n}\times\nabla\times\vec{E}+\gamma_1\hat{n}\times\hat{n}\times\vec{E}=2\gamma_1\hat{n}\times\hat{n}\times\vec{E}^{\rm in}-\hat{n}\times\hat{n}\times\nabla_t E_n=\vec{U}_0. \tag{9}$$

Note that γ_1 in (8) is the complex propagation constant for the two-and-one-half-dimensional uniform-line case, which has been obtained from the precomputation of the two-and-one-half-dimensional edge-element codes. Comparing (9) with (3), we have

$$\begin{aligned}\gamma_p&=\gamma_1\\ \vec{U}&=2\gamma_1\hat{n}\times(\hat{n}\times\vec{E}^{\rm in}).\end{aligned} \tag{10}$$

On O_2, the surface through which the wavefront propagates out of the via structure, we have

$$\vec{E}=T\vec{E}^0(x,y)e^{-\gamma_2(z-z_2)}=\vec{E}^{\rm tr} \tag{11}$$

where T is the transmission coefficient. On O_2, we also have

$$\hat{n}\times\nabla\times\vec{E}+\gamma_2\hat{n}\times\hat{n}\times\vec{E}=-\hat{n}\times\hat{n}\times\nabla_t E_n=\vec{U}_0. \tag{12}$$

Therefore, $\gamma_p=\gamma_2$ and $\vec{U}=0$. On other boundary surfaces, either the boundary conditions of the first or third kind apply. The adjoint field, which satisfies (4) and (5), on O_2 has the form of $\vec{E}^{\rm in\dagger}=\vec{E}_0^{\dagger}e^{\gamma_2(z-z_2)}$. At port 2, we have

$$\begin{aligned}\vec{E}^{\dagger}&=\vec{E}_t^0(x,y)e^{\gamma_2(z-z_2)}+R\vec{E}_t^0(x,y)e^{-\gamma_2(z-z_2)}\\&\quad-\vec{E}_z^0(x,y)e^{\gamma_2(z-z_2)}+R\vec{E}_z^0(x,y)e^{-\gamma_2(z-z_2)}\\&=\vec{E}^{\rm in\dagger}+\vec{E}^{\rm re\dagger}.\end{aligned} \tag{13}$$

Similar to (9), we find

$$\begin{aligned}&\hat{n}\times\nabla\times\vec{E}^{\dagger}+\gamma_2\hat{n}\times\hat{n}\times\vec{E}^{\dagger}\\&\qquad=2\gamma_2\hat{n}\times\hat{n}\times\vec{E}^{\rm in\dagger}-\hat{n}\times\hat{n}\times\nabla_t E_n^{\dagger}=\vec{U}_0^{\dagger}.\end{aligned} \tag{14}$$

On O_1, the adjoint field is governed by

$$\hat{n}\times\nabla\times\vec{E}^{\dagger}+\gamma_1\hat{n}\times\hat{n}\times\vec{E}^{\dagger}=-\hat{n}\times\hat{n}\times\nabla_t E_n^{\dagger}=\vec{U}_0^{\dagger}. \tag{15}$$

III. Edge-Element Procedure

For reasons of simplicity, the isotropic case will be considered. We shall assume that the same shape functions employed for the primary fields can also be used for the adjoint fields. For the edge element with a basic building block, we may express the electrical fields in each small cell as [4]

$$\vec{E}^e=\sum_{i=1}^{12}\vec{N}_i^e E_i^e. \tag{16}$$

After using the Ritz procedure and grouping together all of the relationships in the global coordinate system, we arrive at

$$\begin{aligned}&\{[Z_v^e]+\gamma[Z_z^s]+[Z_{tz}^s]+[Z_{-tz}^s]+\gamma[Z_{(-z)}^s]+\gamma_p[Z_i^q]\}[E]\\&\qquad=2\gamma[Z_z^u][E_t^{\rm in}].\end{aligned} \tag{17}$$

Once (17) has been solved, the distribution of the electrical fields will be obtained.

IV. Excess Capacitance and Inductance

Once the distribution of the 3-D electrical field has been determined, the reflection coefficient can be evaluated from (8). For example, when the system is excited from port 1, we have

$$\Gamma=\left.\frac{\int_{0_1}ds[\vec{E}\cdot\vec{E}^{2D}-\vec{E}^{2D}\cdot\vec{E}^{2D}]}{\int_{0_1}ds\vec{E}^{2D}\cdot\vec{E}^{2D}}\right|_{z=z_1}. \tag{18}$$

Similarly from (11), the transmission coefficient is

$$T=\left.\frac{\int_{0_2}ds\;\vec{E}\cdot\vec{E}^{2D}}{\int_{0_2}ds\;\vec{E}^{2D}\cdot\vec{E}^{2D}}\right|_{z=z_2} \tag{19}$$

provided the field is properly normalized [5]. The scattering parameters of a two-port system are

$$S_{11}=\Gamma\quad S_{21}=T. \tag{20}$$

TABLE I

Generated by Finite Edge Element Method for Through Hole Via Structure				
Frequency, GHz	Reflection, S_{11}	Transmission, S_{21}	Inductance, nH	Capacitance, pF
5	2.56E-3	0.99998	55.767E-3	21.274E-3
10	1.29E-2	0.99986	55.568E-3	24.602E-3
15	2.07E-2	0.99968	55.406E-3	24.965E-3
20	2.77E-2	0.99944	55.204E-3	25.046E-3
25	3.46E-2	0.99910	54.950E-3	25.122E-3
30	4.19E-2	0.99876	54.650E-3	25.254E-3

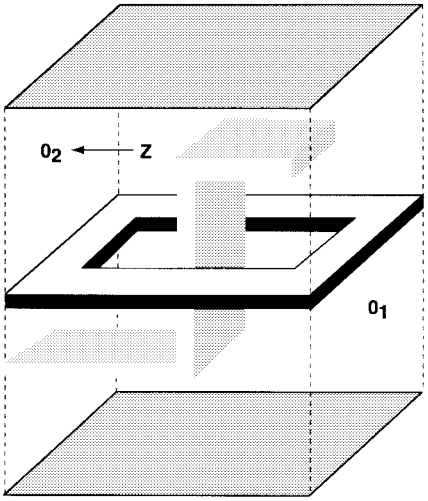

Fig. 1. Via configuration.

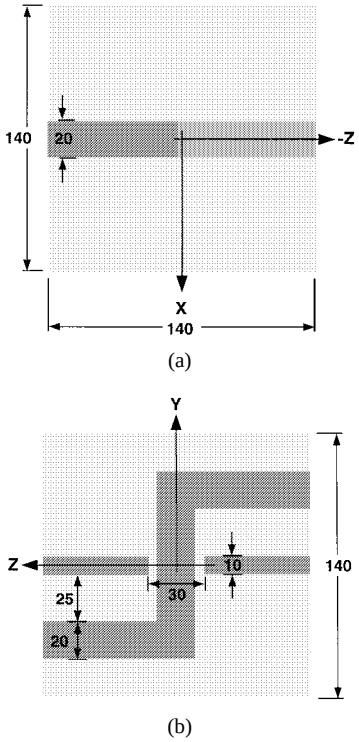

Fig. 2. (a) Top and (b) side views of the through-hole via modeled with finite-edge-element method (FEEM) (all dimensions are in microns).

The Y-parameters can be found from two-port network theory. Based on the Π-type equivalent circuits, we then have the equivalent capacitance and inductance

$$C = \frac{\Im\, Y_{12}}{\omega} \quad L = \frac{1}{\omega\, \Im\, (Y_{11} - Y_{12})}. \tag{21}$$

The resistance and the conductance can be found in the same way. The resistance can be ignored in this equivalent circuit because while the vias are of fairly small cross section, their vertical height between layers is also quite small.

V. Numerical Examples

The nonsymmetric complex sparse system equation (17) was solved using the Harwell subroutines. Only a few minutes are required on an IBM RS-6000 computer for each frequency point, when the total number of unknowns is approximately 3000.

Example 1: Through-hole vias are typically used to connect signal lines residing on different metal layers in most printed-circuit-board technologies and in some multichip module (MCM) technologies. For the circuit design, engineers are concerned about overall signal integrity on interconnects carrying wide-band signals, and thus wish to understand the magnitude of the excess inductance and capacitance caused by this via discontinuity. The method described herein provides the needed parametric values. Note in Table I that the two reference planes incorporated into the via structure, shown in Fig. 1, are placed at locations $z_1 = -0.07$ mm and $z_2 = 0.07$ mm, respectively. Fig. 2(a) and (b) depicts the top and side view of the structure, with all dimensions (in microns) included. The resulting frequency-dependent S-parameters are listed in Table I, where it can be seen that the effect of the via of Fig. 1 on the signal integrity is very minor. Laboratory measurements support this conclusion. The capacitance values are compared with the finite-difference time-domain (FDTD) results, with a discrepancy $\leq 7\%$.

Example 2: An air bridge was modeled using the spectral-domain analysis (SDA) in [6]. We repeated this example using the newly developed edge-element formulation. Good agreement of the S-parameters has been obtained in comparison with the SDA. Due to space limitations, we are not able to include the figure.

VI. Conclusions

In this paper, we have identified an additional term in the boundary condition of the third kind for 3-D structures. In conjunction with the two-dimensional uniform transmission-line results, the newly developed 3-D formulation can extract from impedance discontinuities the reflected and transmitted waves, and convert them

into frequency-dependent lumped-circuit parameters. A numerical example of a through-hole via, typically found in printed circuit boards and MCM's, was analyzed. Comparisons with available published results indicate excellent agreement with this new method.

REFERENCES

[1] J. Tan and G. Pan, "A new edge element analysis of dispersive waveguiding structures," *IEEE Trans. Microwave Theory Tech.*, vol. 43, pp. 2600–2607, Nov. 1995.

[2] J. Wang and R. Mittra, "Finite element analysis of MMIC structures and electronic packages using absorbing boundary conditions," *IEEE Trans. Microwave Theory Tech.*, vol. 42, pp. 441–449, Mar. 1994.

[3] W. C. Chew, *Waves and Fields in Inhomogeneous Media*. New York: Van Nostrand, 1990.

[4] J. Jin, *The Finite Element Methods in Electromagnetics*. New York: Wiley, 1993.

[5] R. E. Collin, *Field Theory of Guided Waves*, 2nd ed. New York: IEEE Press, 1990.

[6] T. B. Becks and I. Wolff, "Analysis of 3-D metallization structures by a full-wave spectral domain technique," *IEEE Trans. Microwave Theory Tech.*, vol. 40, pp. 2219–2227, Dec. 1992.